Self-interaction-corrected pseudopotentials for silicon carbide

Björn Baumeier,* Peter Krüger, and Johannes Pollmann
Institut für Festkörpertheorie, Universität Münster, D-48149 Münster, Germany
(Received 25 May 2005; revised manuscript received 23 February 2006; published 16 May 2006)

We report electronic and structural properties of cubic and hexagonal 3C-, 2H-, 4H-, and 6H-SiC bulk crystals and of the C-terminated SiC(001)-$c(2\times2)$ surface as resulting from density functional theory (DFT) within local density approximation (LDA). In particular, we employ newly constructed nonlocal, norm-conserving pseudopotentials which incorporate self-interaction corrections. Results obtained with usual pseudopotentials show the typical LDA shortcomings, most noticeably the systematic underestimate of the band gap. These problems are attributed to an unphysical self-interaction inherent in the common DFT-LDA. We describe the construction of appropriate self-interaction-corrected pseudopotentials for Si and C atoms and show how they can be transferred to the SiC solid by adequate modifications. It is in the very nature of our pseudopotentials that they cause no additional computational effort, as compared to usual pseudopotentials in standard LDA calculations. To test their transferability to different crystal structures we apply these pseudopotentials to both cubic and hexagonal polytypes of SiC. The resulting energy gaps are in excellent agreement with experimental data and the bulk band structures are in most gratifying agreement with the results of considerably more elaborate quasiparticle calculations. Structural properties of the different polytypes are found in excellent agreement with experiment, as well, not showing the usual LDA underestimate of lattice constants and overestimate of bulk moduli. Also the electronic structure of SiC(001)-$c(2\times2)$, calculated to exemplify the usefulness of the pseudopotentials for surfaces, shows improved agreement with experiment as compared to the respective surface band structure obtained within standard LDA.

DOI: 10.1103/PhysRevB.73.195205 PACS number(s): 71.15.Mb, 71.20.Nr

I. INTRODUCTION

Since the advent of semiconductor technology, Si and silicon-based materials have played a vital role in the development of modern semiconductor devices. At present, however, the physical limits of such devices exclusively based on Si are gradually reached, e.g., the maximum operating temperature of approximately 200 °C which severely limits the applicability of such devices for process control or data logging in many relevant high temperature processes. A more intensive use of silicon carbide compounds is expected to overcome some of these limitations as SiC has a number of favorable properties, among those a high operating temperature (approximately 800 °C) and high mechanical stability.[1]

From a microscopic point of view, SiC is a very unique material.[2] In contrast to homopolar elemental semiconductors, like Si or Ge, it is the only existing heteropolar group-IV compound. Its heteropolarity gives rise to considerably ionic Si—C bonds. Another interesting aspect is the polytypism of SiC.[3] Different polytypes are characterized by the stacking sequence of their constituent Si-C double layers along a certain direction. There are more than 200 known polytypes, with the cubic 3C-SiC and the hexagonal 2H-SiC being the most extreme. All other hexagonal and rhombohedral polytypes show combinations of cubic and hexagonal stacking sequences. The respective band-gap energies range from 2.4 eV in 3C-SiC to 3.3 eV in 2H-SiC.

For applications of SiC in opto- and microelectronic devices a precise knowledge of its electronic properties is essential. From a theoretical point of view, density functional theory using the local density approximation has been established as an extremely useful *ab initio* method to calculate these properties. However, standard LDA calculations typically underestimate critical band structure data, like the band gap or the valence bandwidth.

In order to remedy these deficiencies in the description of electronic properties, several improvements have been developed. For example, quasiparticle approaches based on the *GW* approximation[4,5] (GWA), which treat one-particle excitations using electron Green functions, have been particularly successful in this regard.[6–9] Compared to standard LDA, however, the numerical effort for GWA calculations is considerably higher. This is particularly true when systems with broken translational symmetry are described by large unit cells containing many atoms. In such cases GWA calculations become extraordinarily demanding computationally.

The systematic deviations of DFT-LDA results from experimental data can primarily be traced back to unphysical self-interactions inherent in LDA, as has been shown by Perdew and Zunger.[10] The authors applied a self-interaction correction (SIC) to atomic systems and were able to overcome the shortcomings of the LDA to a large extent. These corrections are state dependent, however, so that a direct transfer of this approach to bulk solids is computationally very demanding. Nevertheless, Svane and Gunnarson[11–14] have performed respective calculations for transition metals using a SIC energy functional, allowing the system to minimize its total energy by forming delocalized, as well as localized states. The authors observed that localization minimizes the total energy. Further results of SIC calculations have been reported by Szotek, Temmerman, and Winter[15–17] for high-T_c superconductors and by Arai and Fujiwara[18] for transition-metal oxides. All these results indicate that the main effect of self-interaction correction originates from localized atomic states. This finding leads us to expect that the introduction of *atomic* and hence localized self-interaction corrections into

state-of-the-art nonlocal, norm-conserving pseudopotentials will approximate the results of full SIC calculations at least to a significant extent.

The idea of incorporating corrections for self-interaction approximately has previously been implemented by various groups in different approaches. First, Rieger and Vogl[19] have reported respective calculations for bulk Si, Ge, Sn, and GaAs. While the authors found significant effects in the description of strongly bound core levels, improvements obtained for the gaps of these s,p bonded semiconductors have only been marginal. Later on, some of the present authors[20–22] have successfully applied a related approach to II-VI semiconductors and group-III nitrides accounting for self-interaction and relaxation corrections (SIRC) in a solid by modified atomic SIC and SIRC pseudopotentials. In the latter work, the relaxation corrections turned out to be of particular importance for the semicore d bands in these compounds. Inspired by this previous work, Filippetti and Spaldin[23] have more recently extended and modified the approach and applied it not only to a II-VI compound and a group-III nitride but also to a number of transition metal and manganese oxides. Their pseudo-SIC approach turned out to work very well for the latter materials, as well. The materials, studied by Vogel *et al.*[20–22] and Filipetti and Spaldin[23] are all characterized by localized semicore d states on which SIC and SIRC have a very pronounced effect.

In this paper, we construct self-interaction-corrected pseudopotentials for the ionic compound semiconductor silicon carbide and investigate their usefulness. It was not obvious *a priori* that the SIC approach leads to quantitative improvements for silicon carbide polytypes, as well, since SiC is a s,p bonded semiconductor and does not have highly localized semicore d states, to begin with. Nevertheless, we find that an appropriate inclusion of self-interaction corrections does improve the description of the bulk electronic and structural properties of SiC polytypes very significantly, indeed. The description of an exemplary SiC surface shows noticeable improvements, as well. Relaxation corrections have only a very minor influence on the band structure of the polytypes and have been ignored, therefore, for simplicity of our approach.

The paper is organized as follows: First, the principles of the construction of SIC pseudopotentials for Si and C are summarized in Sec. II using cubic 3C-SiC as the prototype example for a first application. For this polytype there is the largest set of experimental and theoretical electronic structure data available in the literature for comparison. Next we address structural properties of cubic and hexagonal SiC polytypes in Sec. III. The results of our electronic structure calculations using SIC pseudopotentials for the hexagonal polytypes are then presented in Sec. IV and discussed in comparison with standard LDA results, as well as with GWA results and experiment. Finally, the SiC(001)-$c(2\times2)$ surface is briefly addressed in Sec. V. A short summary concludes the paper.

II. CONSTRUCTION OF SIC PSEUDOPOTENTIALS

In this section, we outline the construction of self-interaction-corrected pseudopotentials and discuss their application in calculations of electronic properties of cubic 3C-SiC, as a prototype example.

A. Standard pseudopotentials

For reference sake, we first very briefly address the standard pseudopotentials which we use in our accompanying LDA calculations. As is well known, electrons from inner core states do not influence chemical bonding in bulk crystals. Therefore, electronic structure calculations can be restricted to the valence electrons accounting for the effects of the core electrons by introducing ionic pseudopotentials. The starting point for constructing usual state-of-the-art *ab initio* pseudopotentials are all-electron LDA calculations for respective atoms. There are several conditions that have to be fulfilled in the construction process, most notably, and also most intuitively, that the all-electron eigenvalues for the atomic valence states are reproduced by the pseudopotentials.[24–26] One characteristic feature of such ionic pseudopotentials is their dependence on angular momentum as

$$\hat{V}^{\mathrm{ps}} = \sum_l V_l^{\mathrm{ps}} \hat{P}_l, \tag{1}$$

where $\hat{P}_l$ is a projection operator on angular momentum eigenstates

$$\hat{P}_l = \sum_m |lm\rangle\langle lm|. \tag{2}$$

These ionic pseudopotentials are semilocal, i.e., nonlocal with respect to the spherical angles ϑ and φ but local with respect to the radial coordinate r, within a chosen core region. They can be separated into a local and a nonlocal part as

$$\hat{V}^{\mathrm{ps}} = \hat{V}^{\mathrm{ps}}_{\mathrm{loc}} + \hat{V}^{\mathrm{ps}}_{\mathrm{nloc}} \tag{3}$$

with

$$\hat{V}^{\mathrm{ps}}_{\mathrm{nloc}} = \sum_l \Delta V_l^{\mathrm{ps}} \hat{P}_l. \tag{4}$$

For practical purposes, it has proven useful to represent the above semilocal pseudopotentials in a fully separable form as proposed by Kleinman and Bylander.[27]

In our standard LDA reference calculations we use the nonlocal, norm-conserving *ab initio* pseudopotentials constructed according to the prescription of Hamann.[26] In all calculations to follow we employ the exchange-correlation potential of Ceperley and Alder,[28] as parametrized by Perdew and Zunger.[10] As basis sets we use Gaussian orbitals with appropriately determined decay constants.[29] In the following construction and first exemplary application of SIC pseudopotentials we use 3C-SiC as a reference. This cubic modification of SiC crystallizes in the zinc-blende structure, with a lattice constant of 4.36 Å. Within standard LDA we obtain the band structure shown in Fig. 1 in direct comparison with a number of experimental data points. It exhibits a heteropolar or ionic band gap between the lowest C 2s-derived band and the three higher s,p-like valence bands as is typical for an ionic compound semiconductor. The total width of the

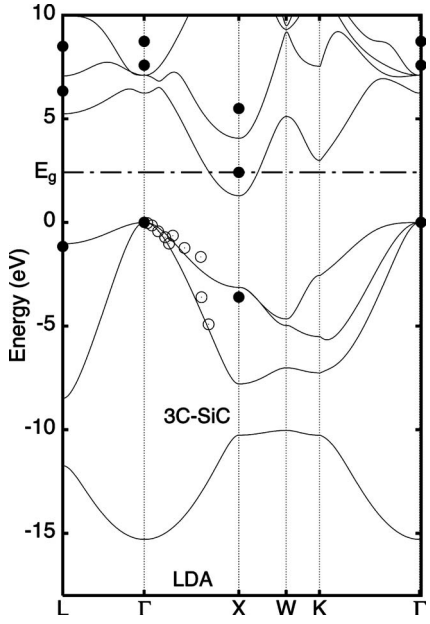

FIG. 1. LDA band structure of 3C-SiC along high-symmetry lines of the Brillouin zone. The dashed line indicates the experimental gap of 2.42 eV (Ref. 30). Open circles show wave vector-resolved photoemission data from Ref. 31. The full dots are derived from optical data. For the respective references, see Table II.

LDA valence bands is 15.29 eV. 3C-SiC has an indirect optical gap between the Γ and the *X* point. The calculated LDA gap energy of 1.29 eV underestimates the experimental value[30] of 2.42 eV by about 45%, as is typical for standard LDA. In addition, the calculated conduction bands show significant **k** dependent deviations from the data points. To the best of our knowledge there are no experimental data available in the literature on the low-lying C 2*s* band.

B. SIC pseudopotentials

The LDA shortcomings of the band structure in Fig. 1 occur in spite of the fact that the employed standard pseudopotentials reproduce by construction the atomic all-electron LDA term values exactly as is shown in Table I, where both the all-electron and the pseudopotential eigenvalues are given. This raises the question how reliable the all-electron LDA results are with respect to experiment. To this end, the experimental ionization energies E_α^{exp} are given for Si and C atoms[32] in Table I, as well. If one interprets the eigenvalues $\epsilon_\alpha^{\mathrm{LDA}}$ as excitation energies, which is usually done, it becomes obvious that they deviate strongly by some 50% from the experimental data. In particular, the measured energy difference between the C 2*p* and Si 3*p* term values of 3.2 eV is strongly underestimated by the respective energy difference of the LDA term values amounting to 1.2 eV, only. Perdew and Zunger[10] have attributed this type of shortcomings in atomic systems to an unphysical self-interaction contained in LDA and have proposed a method to introduce self-interaction corrections of the energy functional, which can be written as

$$E^{\mathrm{SIC}} = E^{\mathrm{LDA}} - \sum_{\alpha}^{\mathrm{occ}} \{E_{\mathrm{Coul}}[\varrho_\alpha] + E_{\mathrm{xc}}^{\mathrm{LDA}}[\varrho_\alpha]\}. \tag{5}$$

Minimization of the energy according to Eq. (5) yields the equivalent to the Kohn-Sham equations

$$\{-\nabla^2 + V_{\alpha,\mathrm{eff}}^{\mathrm{SIC}}(\mathbf{r})\}\phi_\alpha^{\mathrm{SIC}}(\mathbf{r}) = \epsilon_\alpha^{\mathrm{SIC}}\phi_\alpha^{\mathrm{SIC}}(\mathbf{r}). \tag{6}$$

Within pseudopotential framework the orbital-dependent self-interaction corrected effective potential reads

$$V_{\alpha,\mathrm{eff}}^{\mathrm{SIC}}([\varrho],[\varrho_\alpha],\mathbf{r}) = V_\alpha^{\mathrm{ps}} + V_{\mathrm{Coul}}([\varrho],\mathbf{r}) + V_{\mathrm{xc}}^{\mathrm{LDA}}([\varrho],\mathbf{r}) + V_\alpha^{\mathrm{SIC}}([\varrho_\alpha],\mathbf{r}) \tag{7}$$

and

$$V_\alpha^{\mathrm{SIC}}([\varrho_\alpha],\mathbf{r}) = -V_{\mathrm{Coul}}([\varrho_\alpha],\mathbf{r}) - V_{\mathrm{xc}}^{\mathrm{LDA}}([\varrho_\alpha],\mathbf{r}). \tag{8}$$

Here ϱ and ϱ_α are the atomic valence and orbital charge densities, respectively. The solution of Eq. (6) for Si and C pseudoatoms yields the SIC term values $\epsilon_\alpha^{\mathrm{ps,SIC}}$ given in Table I. While there is no exact agreement between the SIC term values and the experimental ionization energies, the deviations from the latter have been reduced dramatically. For example, the energy difference between the C 2*p* and Si 3*p* term values resulting from the SIC calculation as 3.7 eV is in much closer agreement with the experimental value of 3.2 eV than the energy difference between the respective LDA term values of 1.2 eV. Exact agreement was not to be expected, anyway, since we have solved Eq. (6) without including spin polarization because it is insignificant for the SiC solid, to be addressed below. Comparing the term values resulting from the all-electron or pseudopotential LDA calculations with those resulting from the pseudopotential SIC calculations, we first note a pronounced absolute shift of the SIC term values with respect to the LDA term values. Much more importantly, however, the term values resulting from the SIC calculations show prominent relative shifts with respect to one another as compared to the LDA term values. These have very significant bearing on the outcome of electronic structure calculations for solids since the atomic SIC term values of the interacting atoms in the solid occur at largely different relative positions from the start, as compared to the respective LDA term values. So the solid state interaction of the different atoms is strongly influenced thereby giving rise to changes in the energy positions and dispersions of the bulk bands.

TABLE I. Atomic term values (in eV) for C and Si atoms as resulting from nonspinpolarized LDA and SIC calculations. For reference we show both the all-electron and pseudopotential term values resulting in LDA, as well as the energy shifts $\Delta\epsilon_\alpha = \epsilon_\alpha^{\mathrm{ps,SIC}} - \epsilon_\alpha^{\mathrm{ps,LDA}}$ of the eigenvalues due to self-interaction correction.

	E_α^{exp}	$\epsilon_\alpha^{\mathrm{ae,LDA}}$	$\epsilon_\alpha^{\mathrm{ps,LDA}}$	$\epsilon_\alpha^{\mathrm{ps,SIC}}$	$\Delta\epsilon_\alpha$
C 2*s*		−13.7	−13.7	−19.7	−6.0
C 2*p*	−11.3[a]	−5.4	−5.4	−11.1	−5.7
Si 3*s*		−10.9	−10.9	−15.1	−4.2
Si 3*p*	−8.1[a]	−4.2	−4.2	−7.4	−3.2

[a]From Ref. 32.

The *atomic* SIC pseudopotentials for Si and C ions are defined according to Eq. (7) by

$$V_\alpha^{\mathrm{ps,SIC}}([\varrho_\alpha],\mathbf{r}) := V_\alpha^{\mathrm{ps}}(\mathbf{r}) + V_\alpha^{\mathrm{SIC}}([\varrho_\alpha],\mathbf{r}). \tag{9}$$

Next, we have to modify these atomic SIC pseudopotentials such that they can meaningfully be applied to solids. (For details, see Ref. 21.) They feature an asymptotic $-2/r$ tail originating from the Coulomb potential $V_\alpha^{\mathrm{SIC}}([\varrho_\alpha],\mathbf{r})$. Such long-range tails would cause an unphysical overlap of the SIC potential contributions, which are introduced as truly atomic properties in our approach, after all, from different atomic sites. To reduce the overlap of the final correction potentials in the solid we refer all correction potentials relative to the energetically highest atomic state and cut off the $-2/r$ tails appropriately. The energetically highest atomic state is Si $3p$ in the case of SiC. So we rigidly shift all correction potentials accordingly by the same value $V_{\mathrm{shift}} := \epsilon_{\mathrm{Si}3p}^{\mathrm{LDA}} - \epsilon_{\mathrm{Si}3p}^{\mathrm{SIC}} = 3.2$ eV (see $\Delta\epsilon_\alpha$ for Si $3p$ in Table I). Note that the relative distances of the term values, as resulting from the atomic SIC calculations, are not changed thereby so that the physics of the atomic levels remains to be described much more rigorously from the start than by the usual LDA term values. Actually, if the atomic self-interaction corrections $V_\alpha^{\mathrm{SIC}}([\varrho_\alpha],\mathbf{r})$ would directly be applied in a solid state calculation *all* states would experience a strong SIC correction. However, delocalized states are only weakly affected by self-interaction corrections, if at all (see, e.g., Refs. 11–18). This is especially true for atomic states that contribute to the conduction bands of a semiconductor. These are usually the highest *atomic* valence states. We therefore refer all correction potentials relative to the Si $3p$ state. This shift of all atomic SIC potentials by the same amount does not change the relative distances between the atomic SIC levels but reduces the overlap of the final potentials in the solid substantially (see, e.g., Fig. 3 in Ref. 21). By this modification, the influence of the Si $3p$ self-interaction correction is reduced to a large extent in accord with the fact that delocalized conduction-band states themselves do not experience a significant self-interaction. The changes in the band structure are predominantly brought about by the SIC contributions to the C $2s$, C $2p$, and Si $3s$ pseudopotentials. The $-2/r$ tails of the radial components of the correction terms $V_\alpha^{\mathrm{SIC}}([\varrho_\alpha],\mathbf{r})$ are then cut off at suitable radii r_α which we define by the condition that the pseudopotentials with the SIC contributions cutoff at r_α reproduce the atomic SIC term values within 10^{-2} Ry. For the valence states of the Si and C atoms the above criteria yields the radii 3.84 and 4.36 a.u. for C $2s$ and $2p$, and 4.72 and 5.87 a.u. for Si $3s$ and $3p$, respectively. The cutoff is actually achieved on a short length scale by multiplying the correction terms with the smooth function $f(x_\alpha)=\exp(-x_\alpha^7)$ with $x_\alpha = r/r_\alpha$ to avoid problems in their Fourier representation.

The respectively modified self-interaction correction contributions can now be used in the calculations for the solid. For the valence states *of a given ion* they are uniquely specified by the angular momentum quantum number l. They can therefore be written as $V_l^{\mathrm{SIC}}(r)+V_{\mathrm{shift}}$ multiplied by the projector on the angular momentum eigenstates and by the above cutoff function and can simply be added to the nonlocal part of the usual pseudopotentials

$$\hat{V}^{\mathrm{ps,SIC}} = \hat{V}_{\mathrm{loc}}^{\mathrm{ps}} + \hat{V}_{\mathrm{nloc}}^{\mathrm{ps,SIC}} \tag{10}$$

with

$$\hat{V}_{\mathrm{nloc}}^{\mathrm{ps,SIC}} = \hat{V}_{\mathrm{nloc}}^{\mathrm{ps}} + \hat{V}_{\mathrm{nloc}}^{\mathrm{SIC}} = \sum_l \Delta V_l^{\mathrm{ps}} \hat{P}_l + \sum_l \Delta V_l^{\mathrm{SIC}} \hat{P}_l \tag{11}$$

and

$$\Delta V_l^{\mathrm{SIC}}(r) = \{V_l^{\mathrm{SIC}}(r) + V_{\mathrm{shift}}\} f(x_l) \tag{12}$$

with $x_l = r/r_l \equiv r/r_\alpha$.

The nonlocal SIC contributions to the ionic pseudopotentials can now be represented in the fully separable Kleinman-Bylander form

$$\hat{V}_{\mathrm{nloc}}^{\mathrm{SIC}} = \sum_{l,m} \frac{|\phi_{l,m}^{\mathrm{SIC}} \Delta V_l^{\mathrm{SIC}}\rangle \langle \phi_{l,m}^{\mathrm{SIC}} \Delta V_l^{\mathrm{SIC}}|}{\langle \phi_{l,m}^{\mathrm{SIC}} | \Delta V_l^{\mathrm{SIC}} | \phi_{l,m}^{\mathrm{SIC}} \rangle} \tag{13}$$

just as ordinary nonlocal pseudopotentials. The l,m values entering Eq. (13) are uniquely defined by the orbital indices α for each ion.

We conclude this discussion of the construction of SIC pseudopotentials for the solid by noting that we fully incorporate the SIC corrections according to Eq. (12) in our calculations. If one would try, on the contrary, to explicitly incorporate the actual occupation of each band state one would have to construct the SIC pseudopotentials iteratively for the self-consistently changing occupation of the band states. This would necessitate an additional inner self-consistency loop for each $n,\mathbf{k}$ which obviously would render the calculations extremely demanding. Filippetti and Spaldin[23] have considered this alternative. Due to the extremely heavy numerical load involved, however, they do not take the occupation of each particular band state explicitly into account but only a $\mathbf{k}$ space average of the band-state occupations. In addition, they do not construct their pseudopotentials iteratively for each average band occupation anew but construct them once and for all and then weight them by the average band occupation. Using this pragmatic way, the calculations become feasible again in spite of the fact that the actual occupations of the band states are taken into account at least on average. From a general formal point of view this might be somewhat better than the consideration of the band-state occupations in our approach. Yet, the actual results of Filippetti and Spaldin for ZnO and GaN are very similar to our previous results[20–22] so that no conclusive answer as to which approach is better can easily be inferred at present.

The SIC pseudopotentials according to Eqs. (10)–(13) for the silicon carbide solid can now readily be employed in a usual LDA code causing no additional computational effort as compared to a standard LDA calculation. Employing these pseudopotentials for Si and C we obtain the SIC band structure shown in Fig. 2. Compared to the LDA band structure, the fundamental band gap has increased to 2.46 eV and is now in very gratifying agreement with experiment. At the same time, the total width of the valence bands has increased to 17.18 eV. The broadening of the SIC valence bands, as compared to the LDA valence bands, mainly originates from

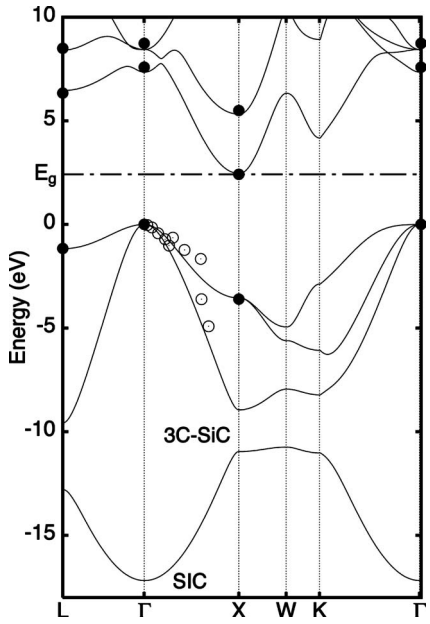

FIG. 2. SIC band structure of 3C-SiC along high-symmetry lines of the Brillouin zone. For further details, see caption of Fig. 1.

the lowering of the C 2*s* band relative to the higher *s*,*p* valence bands due to its stronger self-interaction correction, as already evidenced by the $\Delta\epsilon_\alpha$ value in Table I which is largest for C 2*s*. The dispersion of the measured valence bands along the Γ-*X* line is very well described. In particular, the energy of the highest occupied X_{5v} state, which is observed at −3.60 eV in experiment,[34] is much more accurately described in SIC than in standard LDA (cf. Fig. 1). Most importantly, the SIC approach does not only yield a very good description of the valence bands and the band gap but also a very accurate description of the experimental data for the conduction bands.

In Table II we have summarized band-structure energies for 3C-SiC resulting from our LDA and SIC calculations, as well as theoretical results from two different GWA calculations[8,9] and experimental results[30,33–35] for 3C-SiC. The LDA results show the typical shortcomings discussed above underestimating all conduction-band energies considerably. The SIC results are in very good agreement with the majority of the experimental data. The LDA band-gap problem seems to have largely been overcome by including SIC, at least in this case of 3C-SiC. The overall width of the valence bands resulting from the SIC calculation is larger than that resulting from the GWA calculations of Rohlfing *et al.*[8] but is close to that in the GWA results of Wenzien *et al.*[9] To date there are no experimental data on the total valence bandwidth to compare with. Comparing the GWA results of Wenzien *et al.*[9] with our SIC results, the GWA results from Ref. 8 and the experimental data it appears that the former band-structure energies result in the upper conduction bands significantly higher than all other values. We emphasize this fact already at this point since for the hexagonal SiC polytypes to be discussed below we have only the results of Ref. 9 to compare with.

To further evidence the above difference we summarize in Table III critical point transition energies as resulting from the different calculations in comparison with experimental data. As is most obvious, the LDA values fall far short of all measured transition energies due to the LDA band-gap problem. On the contrary, most of the SIC results and the quasiparticle results from Ref. 8 are in very good accord with the experimental data. The quasiparticle results from Ref. 9 overestimate the transition energies for the reason mentioned above whenever final states in the higher conduction bands are involved.

TABLE II. Calculated band-structure energies (in eV) at high-symmetry points for 3C-SiC in comparison with the results of quasiparticle calculations by Rohlfing *et al.* (Ref. 8) (QPR) and Wenzien *et al.* (Ref. 9) (QPW) and experiment.

3C	LDA	SIC	QPR	QPW	Exp
Γ_{1v}	−15.29	−17.18	−16.44	−17.31	
Γ_{15v}	0.00	0.00	0.00	0.00	0.00
Γ_{1c}	6.25	7.35	7.35	8.29	7.59[a]
Γ_{15c}	7.10	8.45	8.35	9.09	8.74[a]
X_{1v}	−10.25	−10.96	−11.24	−11.82	
X_{3v}	−7.79	−8.95	−8.64	−8.53	
X_{5v}	−3.13	−3.55	−3.62	−3.49	−3.60 [b]
X_{1c}	1.29	2.46	2.34	2.59	2.42[c]
X_{3c}	4.07	5.32	5.59	5.77	5.50[b]
L_{1v}	−11.72	−12.79	−12.75	−13.39	
L_{1v}	−8.49	−9.58	−9.42	−9.39	
L_{3v}	−1.04	−1.17	−1.21	−1.13	−1.16[b]
L_{1c}	5.24	6.46	6.53	7.22	6.34[d]
L_{3c}	7.07	8.41	8.57	8.94	8.50[b]

[a]From Ref. 33.
[b]From Ref. 34.
[c]From Ref. 30.
[d]From Ref. 35.

III. STRUCTURAL PROPERTIES

We now address the question whether the SIC approach yields satisfying results for structural properties, as well.

TABLE III. Calculated critical point transition energies (in eV) in 3C-SiC in comparison with respective results of quasiparticle calculations by Rohlfing *et al.* (Ref. 8) (QPR) and Wenzien *et al.* (Ref. 9) (QPW) and with various values derived from experimental data.

3C	LDA	SIC	QPR	QPW	Exp[a]	Exp[b]
Γ_{1c}-Γ_{15v}	6.25	7.35	7.35	8.29	7.59	7.4
Γ_{15c}-Γ_{15v}	7.10	8.45	8.35	9.09	8.74	9.0±0.2
X_{1c}-X_{5v}	4.42	6.05	5.96	6.08	6.02	5.8
X_{3c}-X_{5v}	7.21	8.91	9.21	9.26	9.10	8.3±0.1
L_{1c}-L_{3v}	6.29	7.63	7.74	8.35	7.50	7.5
L_{3c}-L_{3v}	8.11	9.58	9.78	10.07	9.66	9.4

[a]Derived from the experimental data in Table II.
[b]From Ref. 35.

Here we discuss all four SiC polytypes considered in our work. Structural parameters of solids such as lattice constants or bulk moduli usually result in good agreement with experiment from LDA calculations. Lattice constants are underestimated in the order of 1% and bulk moduli are overestimated often by a somewhat larger percentage. In general, SIC potentials are attractive causing the electrons to be stronger localized around the atomic nuclei. This gives rise to an increased screening of the atomic nuclei leading to an increase in the lattice constants and a decrease in the bulk moduli. Therefore we expect these quantities to result from our approach in even better agreement with the data than from usual LDA calculations.

To determine these parameters we have to calculate the total energy of the system which is a ground-state property. The SIC pseudopotentials allow for an accurate description of the occupied valence bands, as noted above, and should lead to very good total energies, therefore. In the framework of pseudopotential theory the total energy within the full SIC-LDA approach [Eq. (5)] can be written as

$$E^{\mathrm{SIC}} = \sum_{\alpha}^{\mathrm{occ}} \epsilon_{\alpha}^{\mathrm{SIC}} + \Delta E_1 + \Delta E_2 + E_{\mathrm{ion}}, \tag{14}$$

with

$$\Delta E_1 = \int \left(-\frac{1}{2} V_{\mathrm{Coul}}([\tilde{\varrho}],\mathbf{r}) + \epsilon_{\mathrm{xc}}^{\mathrm{LDA}}([\tilde{\varrho}],\mathbf{r}) - V_{\mathrm{xc}}^{\mathrm{LDA}}([\tilde{\varrho}],\mathbf{r}) \right) \tilde{\varrho}(\mathbf{r}) d^3r \tag{15}$$

and

$$\Delta E_2 = \sum_{\alpha}^{\mathrm{occ}} \int \left(\frac{1}{2} V_{\mathrm{Coul}}([\tilde{\varrho}_\alpha],\mathbf{r}) - \epsilon_{\mathrm{xc}}^{\mathrm{LDA}}([\tilde{\varrho}_\alpha],\mathbf{r}) + V_{\mathrm{xc}}^{\mathrm{LDA}}([\tilde{\varrho}_\alpha],\mathbf{r}) \right) \tilde{\varrho}_\alpha(\mathbf{r}) d^3r. \tag{16}$$

Here, $\tilde{\varrho}$ and $\tilde{\varrho}_\alpha$ are the valence and orbital charge densities in the solid, respectively, and E_{ion} is the ion-ion interaction energy. The terms $\Delta E_1 + \Delta E_2$ account for double counting that occurs when the SIC eigenvalues $\epsilon_\alpha^{\mathrm{SIC}}$ are simply summed up. The term ΔE_1 is the usual term accounting for double counting within standard LDA.

In order to evaluate the term ΔE_2, we rewrite it as

$$\Delta E_2 = \sum_{\alpha}^{\mathrm{occ}} \int (V_{\mathrm{Coul}}([\tilde{\varrho}_\alpha],\mathbf{r}) + V_{\mathrm{xc}}^{\mathrm{LDA}}([\tilde{\varrho}_\alpha],\mathbf{r})) \tilde{\varrho}_\alpha(\mathbf{r}) d^3r - \sum_{\alpha}^{\mathrm{occ}} \int \left(\frac{1}{2} V_{\mathrm{Coul}}([\tilde{\varrho}_\alpha],\mathbf{r}) + \epsilon_{\mathrm{xc}}^{\mathrm{LDA}}([\tilde{\varrho}_\alpha],\mathbf{r}) \right) \tilde{\varrho}_\alpha(\mathbf{r}) d^3r. \tag{17}$$

Except for the sign, the term in parantheses in the first line is the solid state analog to the SIC contribution in the atomic effective potential of the Kohn-Sham equations as defined in Eq. (8) while the integral in the second line is the Hartree exchange-correlation energy $E_{\mathrm{HXC}}[\tilde{\varrho}_\alpha]$ of the orbital charge density $\tilde{\varrho}_\alpha$. ΔE_2 then reads

$$\Delta E_2 = -\sum_{\alpha}^{\mathrm{occ}} \int V_\alpha^{\mathrm{SIC}}([\tilde{\varrho}_\alpha],\mathbf{r}) \tilde{\varrho}_\alpha(\mathbf{r}) d^3r - \sum_{\alpha}^{\mathrm{occ}} E_{\mathrm{HXC}}[\tilde{\varrho}_\alpha]. \tag{18}$$

In the SIC pseudopotential approach, we only calculate the valence charge densities $\tilde{\varrho}(\mathbf{r})$ for the solid by solving the Kohn-Sham equations but not the orbital charge densities $\tilde{\varrho}_\alpha$. Therefore, we resort in the same way as in the construction of the SIC pseudopotentials to the modified SIC pseudopotentials $\Delta V_\alpha^{\mathrm{SIC}}$ as defined in Eq. (12) and E_{HXC} as functions of the atomic charge densities ϱ_α and approximate ΔE_2 correspondingly. Projecting the solid-state wave functions onto the localized atomic one-particle orbitals $\phi_\alpha^{\mathrm{SIC}}$, ΔE_2 can be approximated by[21]

$$\Delta E_2 \approx -\sum_{n,\mathbf{k}} \langle \psi_{n,\mathbf{k}} | \hat{V}_{\mathrm{nloc}}^{\mathrm{SIC}} | \psi_{n,\mathbf{k}} \rangle - \sum_{\alpha}^{\mathrm{occ}} E_{\mathrm{HXC}}[\varrho_\alpha] \tag{19}$$

with $\hat{V}_{\mathrm{nloc}}^{\mathrm{SIC}}$ according to Eq. (11).

$E_{\mathrm{HXC}}[\varrho_\alpha]$ is then an atomic property which is constant in the solid and drops out when derivatives of the total energy are calculated.

Using Eq. (14) with the above approximation for ΔE_2 we evaluate the total energy of the investigated systems for a number of unit cell volumes around its minimum and determine the lattice constants and bulk moduli. For comparison we have also calculated these quantities within standard LDA.

The results for the cubic and hexagonal 3C, 2H, 4H, and 6H polytypes are summarized in Table IV. The agreement of the structure parameters with the experimental values is excellent. The lattice constants are underestimated by only 0.3%, at most, while the bulk modulus is underestimated by 0.9% for 3C-SiC and overestimated by 0.4% for 2H-SiC. The agreement of our SIC results with experiment is significantly better than that of the standard LDA results which

TABLE IV. Calculated lattice constants a and c (in Å) and bulk moduli B (in Mbar) of the four investigated SiC polytypes in comparison with experiment (Ref. 37).

		LDA	SIC	Exp
3C	a	4.30	4.35	4.36
	B	2.32	2.22	2.24
2H	a	3.04	3.07	3.08
	c	4.99	5.04	5.05
	B	2.33	2.24	2.23
4H	a	3.04	3.07	3.07
	c	9.95	10.06	10.05
	B	2.34	2.23	
6H	a	3.04	3.07	3.07
	c	14.92	15.07	15.08
	B	2.33	2.24	

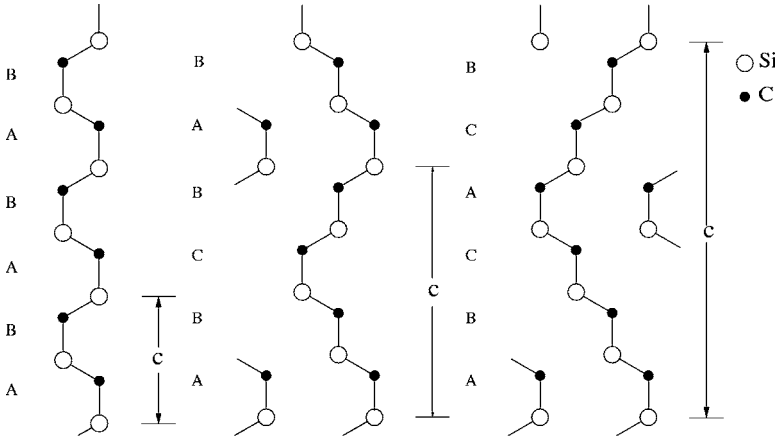

FIG. 3. Stacking sequences in hexagonal polytypes of SiC in [0001] direction. Side views of six Si-C double layers are shown in each case for better comparison.

underestimate the lattice constants up to 1.4% and overestimate the bulk moduli up to 4.5%. The lattice constants and bulk moduli thus result from the SIC calculations about one percent larger and about five percent smaller, respectively, than from LDA. This is due to a stronger increase in the localization of the carbon states, as compared to the Si states, by SIC since the former experience a stronger downward shift in energy by self-interaction correction than the latter (cf. the $\Delta\epsilon_\alpha$ values in Table I and the resulting increase in valence-band width within SIC as evidenced in Fig. 2 and in the third column of Table II). This stronger localization of the C states, as compared to the Si states, gives rise to a weakening of the Si—C bonds which leads to larger lattice constants, as compared to LDA. By the same token, the lattice becomes "weaker" so that the bulk moduli show a decrease in the SIC results, as compared to LDA. This behavior was also observed in other approximate SIC results[19] as well as in the results of full SIC calculations.[14,17]

IV. HEXAGONAL POLYTYPES

Now we address the question whether the very same SIC pseudopotentials used above to calculate the band structure of cubic 3C-SiC work equally well for the band structure of other SiC lattices. To this end, we consider the most common hexagonal 2H, 4H, and 6H polytypes in the following.

Figure 3 shows a two-dimensional representation of the stacking sequences of these three hexagonal polytypes along the [0001] direction. To ease the comparison, we have extended all plots along the [0001] direction to six Si-C double layers, with the actual lengths of the unit cell marked by the hexagonal lattice constants c. The purely hexagonal 2H-SiC exhibits a stacking sequence *ABAB*, in contrast to *ABCB* for 4H-SiC and *ABCACB* for 6H-SiC. Electronic properties are being influenced by the stacking sequence and the related hexagonality of the crystals. The 2H polytype has the largest and the 6H polytype has the smallest hexagonality while the cubic 3C-SiC has no hexagonality at all. Choyke *et al.*[36] have found in experiment that there is a linear dependence between the width of the fundamental gap and the hexagonality of the polytypes. The purely hexagonal 2H-SiC has the largest while cubic 3C-SiC has the smallest energy gap. The position of the conduction band minimum in **k** space and the band splitting at the top of the valence bands are affected by hexagonality, as well.

The experimental lattice constants of 2H-SiC are $a=3.08$ Å and $c=5.05$ Å.[37] Our calculated lattice constants (see Table IV) are very close to these values. The calculated band gap energies for 2H-SiC, as resulting from our LDA and SIC calculations are compared in Table V with the results of quasiparticle calculations and with experiment. The electronic band structure of 2H-SiC as resulting from our SIC calculations is shown in the left panel of Fig. 4. Respective band-structure energies resulting from our LDA and SIC calculations are summarized in Table VI in comparison with the GWA results from Ref. 9. Experimental data for 2H-SiC are very scarce, the only known quantity seems to be the width of the fundamental gap of 3.33 eV,[37] with the minimum of the conduction bands at the K point of the hexagonal Brillouin zone. Our band gap of 3.33 eV calculated with the SIC pseudopotentials happens to exactly agree with the experimental value showing a very significant improvement as compared to the LDA result of 2.12 eV. Since there are four ions per unit cell in 2H-SiC the band structure features eight valence bands. Contrary to cubic 3C-SiC, for which the upper valence band is triply degenerate at the Γ point, hexagonal 2H-SiC features a splitting of the top of the valence bands by 0.14 eV. This is attributed to the hexagonal crystal field which gives rise to doubly degenerate

TABLE V. Calculated band-gap energies (in eV) of the four investigated SiC polytypes in comparison with the results of quasiparticle calculations by Rohlfing *et al.* (Ref. 8) (QPR) and Wenzien *et al.* (Ref. 9) (QPW) and with experiment.

	LDA	SIC	QPR	QPW	Exp.
3C	1.29	2.46	2.34	2.59	2.42[a]
2H	2.12	3.33		3.68	3.33[b]
4H	2.14	3.30		3.56	3.26[b]
6H	1.94	3.08		3.25	3.02[b]

[a]From Ref. 30.
[b]From Ref. 37.

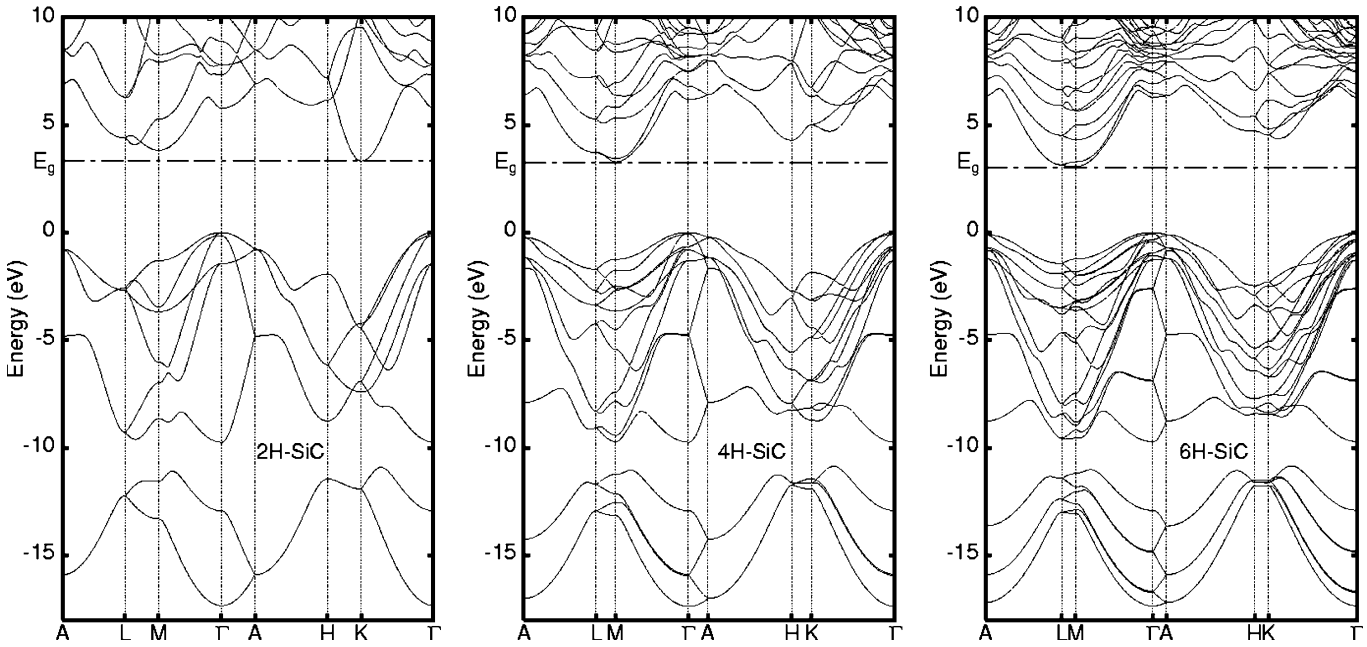

FIG. 4. Band structures of the hexagonal 2H-, 4H-, and 6H-SiC polytypes as resulting from SIC calculations. The respective experimental energy gaps are indicated for reference.

states with p_x and p_y symmetry and a single p_z like state. The valence-band width of 17.35 eV, resulting within SIC, is 1.9 eV larger than that resulting in LDA. Note that it is close to the valence band width of 17.18 eV resulting from our SIC calculations for 3C-SiC. This is, like in the case of 3C-SiC, mostly caused by a strong lowering of the C 2*s* band which is most noticeably around the Γ point. Due to the lack of further experimental data we can only compare our results with the GWA results of Ref. 9. The agreement of the SIC results with the GWA results is quite good, in particular for band-structure energies around the fundamental gap and with respect to the valence-band width. But also in this case the GWA calculations yield higher band-structure energies further up in the conduction bands as was already the case for 3C-SiC (see Table II).

Similarly satisfying results follow for 4H-SiC, which crystallizes with the hexagonal lattice constants[37] $a=3.07$ Å and $c=10.05$ Å. Also in this case our calculated lattice constants are in excellent agreement with these values (see Table IV). The gap energies resulting from our LDA and SIC calculations are compared to GWA results[9] and experiment in Table V. The SIC band structure is shown in the middle panel of Fig. 4 and respective band-structure energies are compared with GWA results from Ref. 9 in Table VII. Also

TABLE VI. Calculated band-structure energies at high-symmetry points of the Brillouin zone for 2H-SiC (in eV) in comparison with the results of quasiparticle calculations by Wenzien *et al.* (Ref. 9) (QPW).

2H	LDA	SIC	QPW
Γ_{1v}	−15.45	−17.35	−17.39
Γ_{6v}	0.00	0.00	0.00
Γ_{1c}	4.60	5.79	6.66
K_{2v}	−3.79	−4.22	−4.12
K_{2c}	2.12	3.33	3.68
H_{3v}	−1.73	−1.93	−1.83
H_{3c}	4.92	6.17	6.86
$A_{5,6v}$	−0.71	−0.77	−0.75
$A_{1,3c}$	5.70	6.94	7.81
M_{4v}	−1.18	−1.30	−1.13
M_{1c}	2.59	3.84	4.28
$L_{1,2,3,4v}$	−2.32	−2.59	−2.30
$L_{1,3c}$	3.16	4.39	4.85

TABLE VII. Calculated band-structure energies at high-symmetry points of the Brillouin zone for 4H-SiC (in eV) in comparison with the results of quasiparticle calculations by Wenzien *et al.* (Ref. 9) (QPW).

4H	LDA	SIC	QPW
Γ_{1v}	−15.45	−17.38	−17.30
Γ_{6v}	0.00	0.00	0.00
Γ_{1c}	5.00	6.20	6.92
K_{2v}	−1.66	−1.86	−1.85
K_{2c}	3.84	5.02	5.45
H_{3v}	−2.45	−2.72	−2.68
H_{3c}	3.10	4.30	4.68
$A_{5,6v}$	−0.21	−0.22	−0.20
$A_{1,3c}$	5.21	6.41	7.14
M_{4v}	−1.11	−1.24	−1.23
M_{1c}	2.14	3.30	3.56
$L_{1,2,3,4v}$	−1.54	−1.71	−1.68
$L_{1,3c}$	2.53	3.72	4.06

TABLE VIII. Calculated band-structure energies at high-symmetry points of the Brillouin zone for 6H-SiC (in eV) in comparison with the results of quasiparticle calculations by Wenzien *et al.* (Ref. 9) (QPW).

6H	LDA	SIC	QPW
Γ_{1v}	−15.42	−17.35	−17.28
Γ_{6v}	0.00	0.00	0.00
Γ_{1c}	5.10	6.30	6.95
K_{2v}	−2.06	−2.30	−2.31
K_{2c}	3.35	4.54	4.88
H_{3v}	−2.26	−2.48	−2.49
H_{3c}	3.54	4.71	5.06
$A_{5,6v}$	−0.10	−0.10	−0.09
$A_{1,3c}$	5.17	6.37	7.02
M_{4v}	−1.09	−1.22	−1.40
M_{1c}	1.94	3.08	3.25
$L_{1,2,3,4v}$	−1.30	−1.45	−1.63
$L_{1,3c}$	1.98	3.15	3.36

for this polytype the band gap of 3.30 eV, calculated with the SIC pseudopotentials, is in very good agreement with the experimental gap of 3.26 eV (see also Table V). The LDA gap of only 2.14 eV strongly underestimates the measured gap, as usual. In 4H-SiC there are eight inequivalent ions per unit cell so that sixteen valence bands result. They are separated from the conduction bands by the fundamental gap which occurs in this case between the Γ and M points. The splitting of the upper valence bands at the Γ point by 0.08 eV is smaller than in 2H-SiC. This is not surprising since 4H-SiC has a smaller hexagonality than 2H-SiC. Hence the crystal field is less pronounced. The total valence-band width of 4H-SiC results from our SIC calculations as 17.38 eV and is very close to the respective value for the 2H polytype. As was the case for 2H-SiC, our SIC band-structure energies for 4H-SiC are in very gratifying agreement with most of the GWA results of Ref. 9 near the gap-energy region. In the higher conduction bands similar deviations as noted above for the 3C and 2H polytypes occur in this case, as well.

Finally, we address 6H-SiC. The measured hexagonal lattice constants are[37] $a=3.07$ Å and $c=15.08$ Å. Our calculated lattice constants are basically identical with these values (see Table IV). The band structure calculated using the SIC approach is shown in the right panel of Fig. 4 and a comparison of our calculated band-structure energies with the GWA results of Ref. 9 is given in Table VIII. As in the other cases above, the band gap of 3.08 eV, calculated using the SIC approach, closely agrees with the experimental value[37] of 3.02 eV (see also Table V) while the respective LDA gap of 1.94 eV is again much too small. In 6H-SiC there are twelve inequivalent ions per unit cell so that twenty-four valence bands result. Their total width of 17.35 eV is basically identical to those of the other two hexagonal polytypes. Due to the further reduced hexagonality of the crystal field, the Γ point splitting of the upper valence bands is only 0.06 eV and thus less pronounced than in both 2H- and 4H-SiC. The band structure of 6H-SiC has one particularly intriguing feature. Unlike the cases of the 2H and 4H polytypes, the exact position of the conduction-band minimum has been a matter of dispute.[9,38,39] Standard LDA calculations yield the conduction-band minimum at a **k** point along the *L*-*M* line. Our SIC calculations, however, yield the minimum at the *M* point as in 4H-SiC, albeit that the lowest conduction band is very flat along the *L*-*M* line. This might be viewed as an indication that it actually does not occur along the *L*-*M* direction. Comparing our SIC results in Table VIII with the GWA results of Ref. 9 very similar conclusions can be drawn as in the case of the 2H and 4H polytypes.

As noted above, there are no experimental data on the valence-band width of the 3C, 2H, and 4H polytypes of SiC. For 6H-SiC, however, King *et al.*[40] have performed x-ray photoemission spectroscopy measurements which are especially useful for assessing the lower valence bands. When we compare the density of states for 6H-SiC resulting from our SIC pseudopotential calculations (not shown for brevity sake) with the measured spectrum we find good agreement for the peaks originating from the lowest C 2*s* band and the following C2*p*-Si3*s* bands, in particular. From this agreement we infer that our calculated valence-band widths for all four polytypes seem to be realistic.

In summary, the SIC pseudopotentials turn out to yield very reliable band-structure energies also for all three considered hexagonal SiC polytypes. In particular, the band gaps of all four polytypes considered resulting from the SIC calculations (see Table V) are in excellent agreement with experiment so that the usual LDA shortcomings in describing gap energies seem to be conquerable entirely at least for the SiC polytypes by taking self-interaction corrections into account.

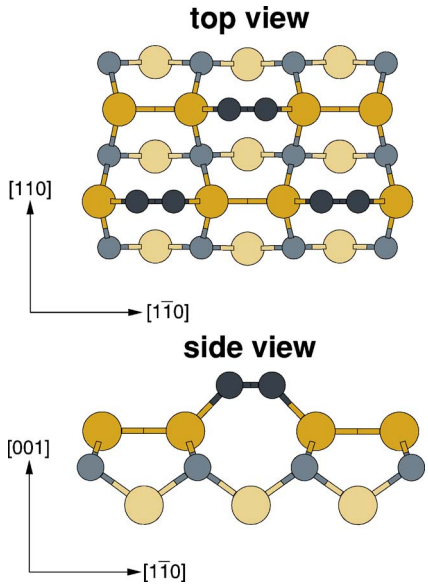

FIG. 5. (Color online) Top and side view of the BDM of the C-terminated SiC(001)-$c(2\times2)$ surface. Top layer carbon atoms in the C≡C surface dimers are shown by small black dots. Third layer C atoms are depicted by small gray (dark gray) circles. Second and fourth layer Si atoms are shown by large dark ocher (dark gray) and large light ocher (light gray) circles, respectively.

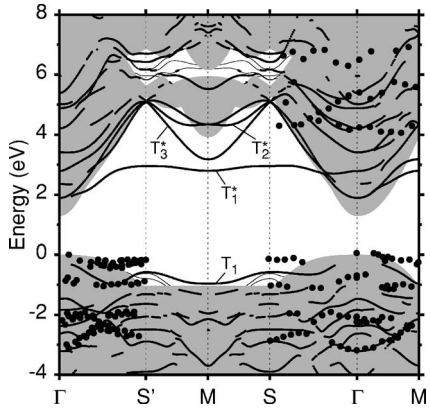

FIG. 6. Surface band structure of the BDM of the C-terminated SiC(001)-$c(2\times2)$ surface as resulting from standard LDA calculations. The gray-shaded areas show the projected bulk band structure. Surface states and resonances are indicated by thick and thin lines. The thick lines refer to pronounced surface states or resonances which are predominatly localized on the first two surface layers. ARPES data from Ref. 44 and ARIPES data from Ref. 45 show measured valence and conduction band states, respectively. ARPES data have not been reported along the S′-M-S line, to date, and ARIPES data have only been measured along the S-Γ-M line.

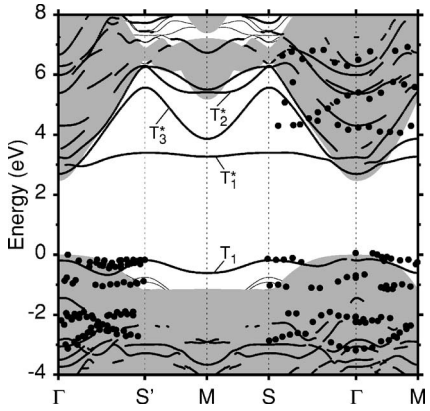

FIG. 7. Surface band structure of the BDM of the C-terminated SiC(001)-$c(2\times2)$ surface as resulting from SIC calculations. For further details, see caption of Fig. 6.

V. 3C-SiC(100)-$c(2\times2)$ SURFACE

Finally, to explore the usefulness of the SIC pseudopotentials for surfaces, we briefly address their application to the C-terminated 3C-SiC(001)-$c(2\times2)$ surface. In particular, there are angle-resolved photoelectron spectroscopy (ARPES) and angle-resolved inverse photoelectron spectroscopy (ARIPES) data available for comparison.

On the basis of a whole body of experimental data and recent *ab initio* DFT calculations there is now general agreement on the bridging-dimer model (BDM) of the 3C-SiC(001)-$c(2\times2)$ surface.[41] Top and side views of the BDM, as resulting from our structure optimization[42] are shown in Fig. 5. Triple-bonded C≡C dimers in the top layer form the main building blocks of this reconstruction (see Fig. 5). We have calculated the surface electronic structure of the BDM employing both standard LDA as well as the SIC pseudopotentials from Sec. II. To describe the surface we use the supercell approach with ten atomic layers (one H, four Si, and five C layers) per supercell. The H layer saturates the C bottom layer of the SiC slab in each supercell to avoid spurious surface states from the bottom layer.

The surface band structure resulting from our LDA calculation is shown in Fig. 6. It basically agrees with the respective surface band structure which we have reported in Ref. 42. Minor differences are due to a number of differences in technical details of the two calculations.[43] We have labeled the most pronounced surface state bands in Figs. 6 and 7 according to Ref. 42. The T_1 band originates from bonding states of the C≡C surface dimers while the T_1^* band originates from the respective antibonding states (cf. respective charge densities in Ref. 42). The T_2^* and T_3^* bands originate from antibonding surface states, as well. Note that the latter two bands coincide with the projected bulk bands of SiC along the Γ-S′ and Γ-S symmetry lines in the LDA surface band structure.

The surface band structure resulting from our SIC calculation is shown in Fig. 7. It shows the same topology of the most salient surface state bands as the LDA surface band structure in Fig. 6. There are significant differences to be noted, however. First and foremost the SIC approach yields an appropriate projected bulk band structure and a realistic projected gap energy region, in particular, at last. The T_1 surface band results slightly higher in energy relative to the projected bulk valence bands than in LDA. The T_1^* band results in the SIC surface band structure throughout most parts of the surface Brillouin zone 0.4 eV higher in energy than in the LDA surface band structure. Note, in particular, that it has moved up in energy by about 1 eV close to the Γ point along the Γ-S' line where it becomes resonant with the projected Si-derived conduction bands. The T_3^* band, which is Si-derived to a considerable extent, is about 0.7 eV higher in energy in the SIC results than in the LDA results. Yet, it remains to be a band of localized surface states within the projected gap also along most of the Γ-S′ and Γ-S symmetry lines. This is due to the fact that the projected bulk conduction bands have shifted up in energy by more than 1 eV as compared to the projected LDA bulk band structure in consequence of the realistic description of the bulk conduction bands within the SIC approach. We have included in Figs. 6 and 7 experimental ARPES and ARIPES data for comparison.

In the ARPES experiments, the measured occupied valence-band states have been referred to the extrinsic Fermi level of the samples used but the doping has not been given in Ref. 44. We have, therefore, aligned the top of the measured bands to the top of the projected bulk valence bands in Figs. 6 and 7. A number of valence-band surface states from the SIC calculations, most noticeably the T_1 dangling-bond band, result in very satisfying agreement with the ARPES data.[44] It might well be that some of the valence-band features observed in experiment are bulk derived since there is no counterpart at all for these features in the calculated surface band structure. The same good overall agreement in the valence bands could also be achieved with the LDA results if the experimental ARPES data were aligned, in view of the lack of knowledge of their absolute energy position, with the T_1 band of the LDA surface band structure at the S′ point, as was done in Ref. 42.

Also the ARIPES data have been referred to the extrinsic Fermi level of the samples used in Ref. 45. In this case the Fermi level position with respect to the valence band maximum has been inferred from other literature data on equally doped samples to be located 1.5 eV above the top of the valence bands. If this assignment is correct we can refer the ARIPES data to the top of the valence bands, as is done in Figs. 6 and 7 without the need of any rigid relative shift. Comparing the two figures it becomes obvious that the lowest empty surface-state band resulting from LDA deviates more strongly from the lowest band determined in ARIPES, actually by 1.3 eV, while this deviation is reduced to 0.9 eV in the SIC surface band structure. In general we note from the comparison that some of the dispersions of the ARIPES data (even if the lowest measured empty band was aligned with the calculated T_1^* band) cannot be reconciled with the theoretical results, neither with the LDA nor the SIC surface band structure.

We conclude from this comparison that the surface band structure of 3C-SiC(001)-$c(2\times2)$, calculated within the SIC approach, shows general improvements over the standard LDA surface band structure concerning the projected bulk band structure and the projected gap, in particular, the absolute energy positions of empty surface-state bands, the character of localized surface states (most noticeably the band T_3^*) and the antibonding T_1^* band which is in somewhat better agreement with experiment. Certainly, these improvements are less impressive than those for the bulk band structures of the SiC polytypes discussed above. The fact that the upward shift of the T_1^* band resulting within SIC, as compared to LDA, is relatively small (only 0.4 eV) ought largely to be due to the fact that the occupied T_1 and the empty T_1^* bands both originate from the triple-bonded C$\equiv$C surface dimers and thus are mainly derived from bulk states in the upper valence bands. These are not influenced dramatically by SIC, as we have seen in Sec. II, so that the improvements in the calculated band gap and conduction bands of 3C-SiC do not fully affect the T_1^* band position by the same upward shift in energy. To the best of our knowledge, there are no GWA results for this surface available in the literature, to date, which could be used for further comparison. A better example for showing pronounced SIC effects on empty surface states would certainly be the relaxed cubic 3C-SiC(110)-(1×1) surface which features an occupied C-derived dangling-bond band near the top of the valence bands and an empty Si-derived dangling-bond band near the bottom of the conduction bands.[46] So the latter can be expected to show a similar upward shift in energy as the bulk conduction bands (mainly Si-derived) when calculated within the SIC approach. Nevertheless we refrained from selecting that example since there are no experimental surface spectroscopy data available in the literature on 3C-SiC(110)-(1×1).

VI. SUMMARY

In this paper we have shown how atomic self-interaction corrections can be incorporated in the nonlocal part of ionic Si and C pseudopotentials to be used in bulk and surface calculations. Within DFT calculations we have applied these SIC pseudopotentials to the most commonly considered cubic and hexagonal polytypes of silicon carbide and have shown that the typical LDA shortcomings in the description of the electronic band structure of these polytypes can almost entirely be overcome. From the comparison of our results with experimental data and other theoretical results from the literature we arrive at the conclusion that SIC pseudopotentials are most suitable for electronic structure calculations. Our results have been achieved without any extra computational effort compared to standard LDA calculations, much in contrast to GWA calculations. In particular in view of this fact, the reached agreement with literature data from experiment and GWA calculations is highly satisfactory and emphasizes that our approach to account for self-interaction corrections is a powerful tool for a more accurate description of the electronic properties of 3C-, 2H-, 4H-, and 6H-SiC bulk crystals. In addition, we have found that structural parameters, such as lattice constants and bulk moduli, derived from total energies calculated employing the SIC pseudopotentials, result in excellent agreement with experiment. Finally, we have shown for an exemplary case that the SIC approach also yields a number of general improvements in the description of surface electronic states, as compared to standard LDA.

ACKNOWLEDGMENTS

The total energy minimization calculations were carried out on the computers of the Morfeus-GRID at the Westfälische Wilhelms-Universität Münster using Condor (see Ref. 47).

*Electronic address: baumeier@uni-muenster.de

[1] *Silicon Carbide, Fundamental Questions, and Applications to Current Device Technology*, edited by W. J. Choyke, H. Matsunami, and G. Pensl (Springer, Berlin, 2004).

[2] W. R. L. Lambrecht, S. Limpijumnong, S. N. Rashkeev, and B. Segall, Phys. Status Solidi B **202**, 5 (1997).

[3] F. Bechstedt, P. Käckell, A. Zywietz, K. Karch, B. Adolph, K. Tenelsen, and J. Furthmüller, Phys. Status Solidi B **202**, 35 (1997).

[4] L. Hedin, Phys. Rev. **139**, A796 (1965).

[5] L. Hedin and S. Lundqvist, in *Solid State Physics*, Vol. 23, edited by F. Seitz, D. Turnbull, and H. Ehrenreich (Academic, New York, 1965).

[6] M. S. Hybertsen and S. G. Louie, Phys. Rev. B **32**, 7005 (1985).

[7] M. S. Hybertsen and S. G. Louie, Phys. Rev. B **34**, 5390 (1986).

[8] M. Rohlfing, P. Krüger, and J. Pollmann, Phys. Rev. B **48**, 17791 (1993).

[9] B. Wenzien, P. Käckell, F. Bechstedt, and G. Cappellini, Phys.

Rev. B **52**, 10897 (1995).
[10] J. P. Perdew and A. Zunger, Phys. Rev. B **23**, 5048 (1981).
[11] A. Svane and O. Gunnarsson, Phys. Rev. B **37**, 9919 (1988).
[12] A. Svane and O. Gunnarsson, Phys. Rev. Lett. **65**, 1148 (1990).
[13] A. Svane, Phys. Rev. Lett. **68**, 1900 (1992).
[14] A. Svane, Phys. Rev. Lett. **72**, 1248 (1994).
[15] Z. Szotek, W. M. Temmerman, and H. Winter, Phys. Rev. B **47**, R4029 (1993).
[16] W. M. Temmerman, Z. Szotek, and H. Winter, Phys. Rev. B **47**, 1184 (1993).
[17] Z. Szotek, W. M. Temmerman, and H. Winter, Phys. Rev. Lett. **72**, 1244 (1994).
[18] M. Arai and T. Fujiwara, Phys. Rev. B **51**, 1477 (1995).
[19] M. M. Rieger and P. Vogl, Phys. Rev. B **52**, 16567 (1995).
[20] D. Vogel, P. Krüger, and J. Pollmann, Phys. Rev. B **52**, R14316 (1995).
[21] D. Vogel, P. Krüger, and J. Pollmann, Phys. Rev. B **54**, 5495 (1996).
[22] D. Vogel, P. Krüger, and J. Pollmann, Phys. Rev. B **55**, 12836 (1997).
[23] A. Filippetti and N. A. Spaldin, Phys. Rev. B **67**, 125109 (2003).
[24] D. R. Hamann, M. Schlüter, and C. Chiang, Phys. Rev. Lett. **43**, 1494 (1979).
[25] G. B. Bachelet, D. R. Hamann, and M. Schlüter, Phys. Rev. B **26**, 4199 (1982).
[26] D. R. Hamann, Phys. Rev. B **40**, 2980 (1989).
[27] L. Kleinman and D. M. Bylander, Phys. Rev. Lett. **48**, 1425 (1982).
[28] D. M. Ceperley and B. J. Alder, Phys. Rev. Lett. **45**, 566 (1980).
[29] We use the decay constants of 0.18, 0.50, 1.00 and 0.25, 1.00, 2.86 (in atomic units) for Si and C, respectively.
[30] R. G. Humphreys, D. Bimberg, and W. J. Choyke, Solid State Commun. **39**, 163 (1981).
[31] H. Hoechst and M. Tang, J. Vac. Sci. Technol. A **5**, 1640 (1987).
[32] C. E. Moore, *Atomic Energy Levels*, Natl. Bur. Stand. (U.S.) Circ. No. 467 (U.S. GPO, Washington, DC, 1949), Vol. I; Vol. II; Vol. III.
[33] W. R. L. Lambrecht, B. Segall, M. Suttrop, M. Yoganathan, R. P. Devaty, W. J. Choyke, J. A. Edmond, J. A. Powell, and M. Alouani, Appl. Phys. Lett. **63**, 2747 (1993).
[34] *Semiconductor Physics of Group IV Elements and III-IV Compounds*, edited by K.-H. Hellwege and O. Madelung, Landolt-Börnstein New Series (Springer, Berlin, 1982).
[35] W. R. L. Lambrecht, B. Segall, M. Yoganathan, W. Suttrop, R. P. Devaty, W. J. Choyke, J. A. Edmond, J. A. Powell, and M. Alouani, Phys. Rev. B **50**, 10722 (1994).
[36] W. J. Choyke, D. R. Hamilton, and L. Patrick, Phys. Rev. **133**, A1163 (1964).
[37] *Properties of Silicon Carbide*, edited by G. L. Harris, EMIS Datareviews No. 13, INSPEC, London, 1995.
[38] C. H. Park, B. H. Cheong, K. H. Lee, and K. J. Chang, Phys. Rev. B **49**, 4485 (1994).
[39] P. Käckell, B. Wenzien, and F. Bechstedt, Phys. Rev. B **50**, 10761 (1994).
[40] S. King, M. C. Benjamin, R. J. Nemanich, R. F. Davis, and W. R. L. Lambrecht, Mater. Res. Soc. Symp. Proc. **395**, 375 (1996).
[41] For a recent review, see J. Pollmann and P. Krüger, J. Phys.: Condens. Matter **16**, S1659 (2004).
[42] F.-H. Wang, P. Krüger, and J. Pollmann, Phys. Rev. B **66**, 195335 (2002).
[43] The calculations of the surface band structure reported in this work and those in Ref. 42 slightly differ concerning the basis sets, the standard pseudopotentials and the number of SiC layers (9 versus 12) per supercell.
[44] H. W. Yeom, M. Shimomura, J. Kitamura, S. Hara, K. Tono, I. Matsuda, B. S. Mun, W. A. R. Huff, S. Kono, T. Ohta, S. Yoshida, H. Okushi, K. Kajimura, and C. S. Fadley, Phys. Rev. Lett. **83**, 1640 (1999).
[45] R. Ostendorf, C. Benesch, M. Hagedorn, H. Merz, and H. Zacharias, Phys. Rev. B **66**, 245401 (2002).
[46] M. Sabisch, P. Krüger, and J. Pollmann, Phys. Rev. B **51**, 13367 (1995).
[47] M. J. Litzkow, M. Livny, and M. W. Mutka, *Condor—A Hunter of Idle Workstations*, in Proceedings of the 8th International Conference on Distributed Computing Systems (IEEE Comput. Sci. Press, Washington, DC, 1988), pp. 104–111.